UC Berkeley

UC Berkeley Previously Published Works

Title

Spatio-temporal ablation dynamics and plasma chemistry of aluminum induced by temporally modulated ytterbium fiber laser

Permalink

https://escholarship.org/uc/item/3fg945vf

Journal

Applied Physics Letters, 119(22)

ISSN

0003-6951

Authors

Park, Minok
Balkey, Matthew M
Mao, Xianglei
et al.

Publication Date

2021-11-29

DOI

10.1063/5.0076527

Peer reviewed

eScholarship.org Powered by the California Digital Library
University of California

Applied Physics Letters ACCEPTED MANUSCRIPT

This is the author's peer reviewed, accepted manuscript. However, the online version of record will be different from this version once it has been copyedited and typeset.

PLEASE CITE THIS ARTICLE AS DOI: 10.1063/5.0076527

Spatio-temporal ablation dynamics and plasma chemistry of aluminum induced by temporally modulated ytterbium fiber laser

Minok Park[1,2,3], Matthew M. Balkey[4], Xianglei Mao[1], Costas P. Grigoropoulos[2,3,*], and Vassilia Zorba[1,3,*]

[1]Laser Technologies Group, Energy Technologies Area, Lawrence Berkeley National Laboratory, Berkeley, CA 94720, USA
[2]Laser Thermal Laboratory, Department of Mechanical Engineering, University of California at Berkeley, Berkeley, CA 94720-1740, USA
[3]Department of Mechanical Engineering, University of California at Berkeley, Berkeley, CA, 94720-1740, USA
[4]Sandia National Laboratories, PO Box 5800, Mail Stop 0791, Albuquerque, NM 87185-0791, USA

*Corresponding authors: vzorba@lbl.gov, cgrigoro@berkeley.edu

Abstract

In this work, we studied single-pulse ablation dynamics of temporally modulated continuous wave laser-material interaction with Al using *in situ* multimodal time-resolved diagnostics, that describe in detail the associated physical and chemical processes. Time-resolved scattering, emission imaging, and optical emission spectroscopy unveiled a sequence of events spread out across three distinct phases: (i) early phase ablation process, associated with particle generation and liquid Al columns formation (< 20 μs), (ii) secondary detonation when sufficient ejected material is accumulated over the surface (20-50 μs), and (iii) molten liquid Al pool oscillation on the surface, followed by large droplet ejection from the liquid pool (100-500 μs). Atomic Al and AlO were observed with optical emission spectroscopy at different ratios during the entire lifetime of the event, verifying the formation of oxidized Al vapor upon its interaction with air. Morphological and compositional characterization confirmed surface oxidation and material re-solidification in the form of protrusions produced during the irradiation process. This work provides insights into the complex physical and chemical mechanisms of single-pulse ablation in the sub-millisecond laser pulse regime, which are critically important for parameter optimization in a variety of laser processing, microfabrication, and deposition applications.

Laser ablation is currently employed in many applications, such as surface drilling[1,2], patterning[3], and nanoparticle (NPs) synthesis[4,5], due to its versatility and ability to provide single-step, chemical-free processing protocols. Short-pulse calculated lasers, such as femtosecond (fs) lasers, have been extensively explored for precise ablation features originating from suppressed thermal effects and minimized heat affected zones.[2,6] Continuous-wave (CW) fiber lasers, on the other hand, are of particular interest due to their ability to remove large amounts of material via deep melting processes, which lead to rapid processing times.[7]

However, the use of such lasers has been limited to materials with relatively low thermal conductivity, such as stainless steel (~14.4 $Wm^{-1}K^{-1}$ at 293 K). Ablation of materials with high thermal conductivity (e.g., aluminum (Al) ~ 236 $Wm^{-1}K^{-1}$, copper ~ 401 $Wm^{-1}K^{-1}$, gold ~ 318 $Wm^{-1}K^{-1}$, and silver ~ 428 $Wm^{-1}K^{-1}$ at 273 K), requires much higher CW laser power because the absorbed heat is diffused into the bulk before the surface temperature reaches the critical temperature for material ejection. Necessarily, a significant amount of re-solidified materials is formed[8] near the irradiated spot due to a long heat diffusion length (~300 μm with an Al thermal diffusivity 95 $\times 10^{-6}$ m^2/s for 1 ms), which is undesirable for precise control of ablated features.

Temporal modulation of the CW laser energy in the kHz repetition rate regime (quasi-CW) has been proposed to augment the amount of material removals and the quality of ablated features via excitation of thermo-capillary driven oscillating surface waves.[8] Due to the short duration of the modulated pulse compared to the lifetime of the ablation process, multiple pulses interact with the molten material generated by the preceding pulses, to enhance liquid material removal.

In addition to interdepended physical processes[9,10] (plasma plumes, nano-/micro- particles, liquid phase expulsion[9]), chemical transformations and new species formation in the laser-induced plasma state may play a pivotal role in the ablation process. Therefore, a fundamental-level understanding of the complex underlying physical and chemical mechanisms is needed to control and optimize processes for aforementioned applications.

In this Letter, we explored the ablation dynamics of Al induced by a single sub-millisecond laser pulse from a temporally modulated CW ytterbium (Yb) fiber laser. A suite of multimodal diagnostics was setup around the laser-material interaction site to probe in real-time the complex ablation process dynamics and chemistry, across different timescales. Specifically, scattering imaging across 500-930 nm was utilized to examine the ejection of NPs and liquid Al columns. Emission imaging only (without the probe laser) was utilized to analyze the detonation of accumulated liquid Al, propagating Al vapor, plasmas, and ejected bulk droplets. Additionally, optical emission spectroscopy was used to analyze the chemical composition of Al plasmas. The combination of technologies with *ex-situ* surface

Applied Physics Letters ACCEPTED MANUSCRIPT
This is the author's peer reviewed, accepted manuscript. However, the online version of record will be different from this version once it has been copyedited and typeset.
PLEASE CITE THIS ARTICLE AS DOI: 10.1063/5.0076527
AIP Publishing

morphology characterizations provides insights into the physics and chemistry of single-pulse ablation in the with sub-millisecond laser pulses.

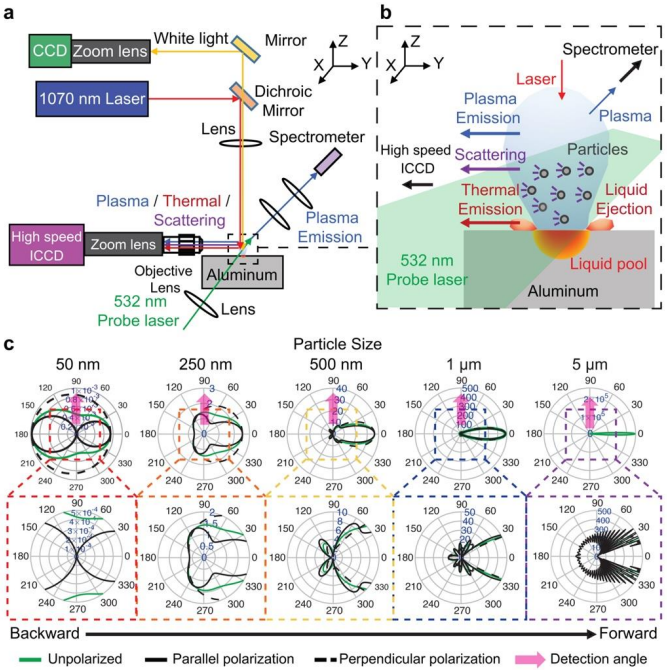

Figure 1. (a) Optical setup for time resolved emission and scattering imaging with the ICCD and high-speed camera. The temporally modulated 1070 nm, 500 μs pump laser interacts with the sample in the normal direction. A 532 nm CW probe laser is used for time-resolved scattering imaging, and thermal and plasma induced emission are utilized for emission imaging (500-930 nm). (b) Schematic of techniques used to probe the plasma plume, nano-/micro-particles, and the liquid pool. (c) Angular distribution of scattered light calculated by Mie theory for Al.

Figure 1 (a) illustrates the optical setup used to study the ablation processes in air under atmospheric conditions. Specifically, single pulses (500 μs pulse duration, 1070 nm wavelength, and M^2 = 1.05 beam quality) of the Yb fiber laser (YLR-150/1500-QCW-AC, IPG photonics) were focused by a convex lens (f = 150 mm) on fresh spots of the sample in the normal direction, yielding a 30 μm beam diameter. A laser peak power of 1400 W (= 1.98×10^8 W/cm^2) was used for the purposes of this work. An Al substrate with 1 mm in thickness (Sigma Aldrich, purity 99 %) was utilized as a target without polishing.

To investigate the dynamics of the ejected species up to the NIR spectral range, we implemented time-resolved combined scattering and emission imaging with a 532 nm CW probe laser (Laserglow Technologies), coupled with an Intensified Charged Coupled Device (ICCD) camera (PI-MAX2, Princeton Instrument). The imaging system was equipped with 3X and 10X objective lenses which provided different fields of view to capture the entire material ejection dynamics across different times (**Fig. 1 (a)-(b)**).

The design of the scattering system was based on Mie scattering analysis which provided information about angular distribution of the scattered light. Side scattering was chosen to avoid enhanced forward scattering by large particles and directly transmitted probe laser radiation[11]. The 532 nm probing wavelength was selected upon considering the spectral dependence of the predicted angular scattering distributions. The complex refractive index of Al (n = 0.91 and k = 6.28 at 532 nm)[12] was used for the Mie calculations shown in **Fig. 1 (c)**. Based on these findings, the probe laser was focused by a convex lens (f = 100 mm) at 90 degrees which is perpendicular to the detection angle.

Applied Physics Letters ACCEPTED MANUSCRIPT
This is the author's peer reviewed, accepted manuscript. However, the online version of record will be different from this version once it has been copyedited and typeset.
PLEASE CITE THIS ARTICLE AS DOI: 10.1063/5.0076527

The power of the probe laser was adjusted at 0.5 W to probe liquid Al, and 0.9 W to probe the NPs, in order to prevent pixel saturation of the ICCD camera.

Time-resolved emission imaging was performed on the identical setup without the probe laser, to capture emission from plasma plumes and thermal emission from liquid Al in the 500-930 nm spectral range filtered by a spectral filter (FESH0950, Thorlabs). Emission spectra were acquired to correlate ejection dynamics with plasma chemistry. Spectral emission was collected by two convex lenses and focused into an optical fiber coupled to a spectrometer (IsoPlane, Princeton Instruments) which was equipped with an ICCD detector (PI-MAX3, Princeton Instrument).

The ICCD temporal resolution was tuned between 100 ns – 5 µs to match the timescale of the relevant material ejection processes. Note that 0.4 µs the shortest gate delay achieved due to the synchronization between each of the diagnostic system components and the pump laser. Separately, a high-speed CMOS camera (FASTCAM Mini UX50, Photron) with a temporal resolution of 20 µs (50,000 fps) was used for complementary measurements of the ejection dynamics at later times. To ensure consistency and reproducibility, every measurement is performed at a fresh sample location and was separately repeated 3 times. Following laser irradiation, the sample surface morphology was characterized using white light interferometry (WLI) and scanning electron microscopy (SEM). The sample elemental composition was verified with energy-dispersive X-ray spectroscopy (EDS).

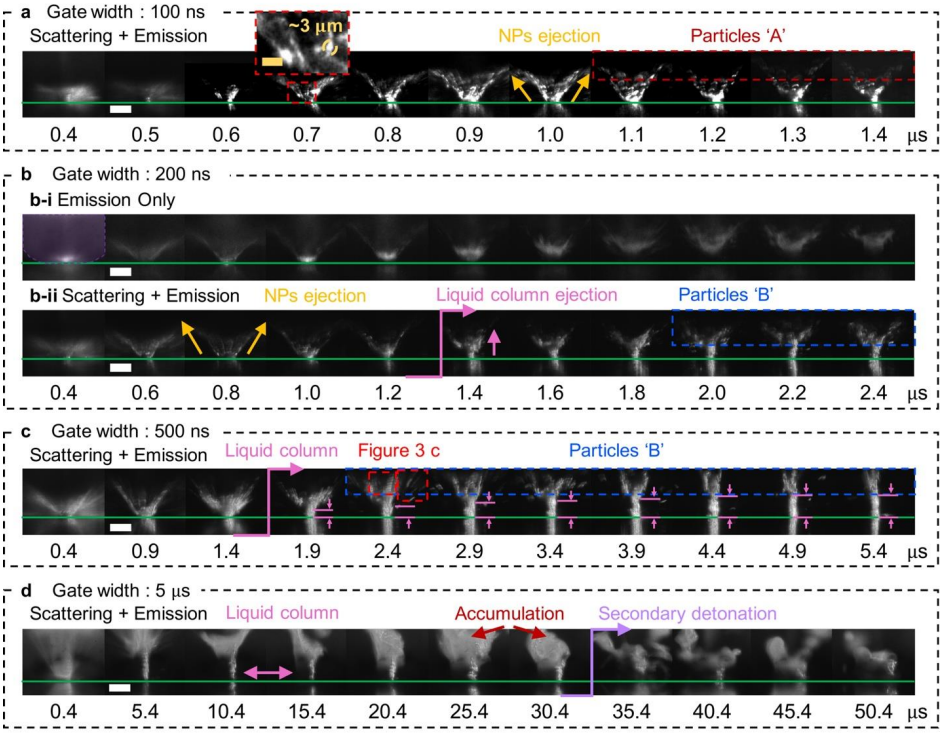

Figure 2. Early-phase material ejection up to 50.4 µs after the laser hits the surface. Time-resolved scattering images were acquired with (a) 100 ns, (b) 200 ns, (c) 500 ns, and (d) 5 µs gate width at each time delay. The green horizontal line represents the target surface. The insets show magnified views of corresponding images. The white scale bar is 50 µm, and the yellow scale bar is 10 µm.

Figure 2 shows time-resolved scattering images captured at different delay and gate times covering a time range from 400 ns to 50.4 µs after the laser pulse, at different gate width increments (100 ns to 5 µs). The green lines

Applied Physics Letters ACCEPTED MANUSCRIPT
This is the author's peer reviewed, accepted manuscript. However, the online version of record will be different from this version once it has been copyedited and typeset.
PLEASE CITE THIS ARTICLE AS DOI: 10.1063/5.0076527
AIP Publishing

represent the target surface of Al and the areas below are mirror images of the ejected material off of the reflective Al surface. Emission images (**Fig. 2 (b-i)**) were obtained without the probe laser to compare with the scattering images (**Fig. 2 (b-ii)**).

In the early ablation process up to 1.4 µs after the laser pulse interacts with the sample (**Fig. 2 (a)**), streak lines appeared in the scattering images at oblique angles (yellow arrows). These are attributed to particle ejection. From Mie theory modeling (**Fig. 1 (c)**), the relative intensity of the side-scattered light is a function of their corresponding size and density, and becomes weaker as the particle diameter decreases. Considering that some of the smallest distinct particles detected in the scattering images have a ~3 µm diameter (inset-shown in the red rectangle), we can assume that the sizes of the ejected particles which make up the streak lines are likely of the order of hundreds of nanometers. We call these types of particles [particles 'A']. These streak lines become less intense with time, which can be attributed to (i) reduced particle density in the expanding plasma, and (ii) the fact that the NPs propagate out of the depth of field of the objective lens (3.5 µm), leading to fainter particle silhouettes (1.4 µs, **Fig. 2 (a)**).

Previous work on femtosecond laser irradiation, has shown that the presence of pressurized plasma plumes may drive the motion of NPs to oblique angles due to the Gaussian spatial distribution of the laser, with a higher local laser intensity in the center as compared to the peripheral areas.[10] Likewise, in the case of temporally modulated CW pulses we observed extended emitting plumes at 0.4 µs after the pulse in **Fig. 2 (b-i)**, with the purple dotted line showing the outline of the expanding plasma. Although we were unable to probe the early plasma evolution before 0.4 µs due to temporal synchronization limitations, it is very likely that the plume initially formed at the center of the laser and the pressurized plume pushed particles towards the periphery, in accordance to observations with other laser sources[10, 13, 14].

For the chosen temporal modulation (500 µs), the laser continues interacting with the ejected material volume continuously over the duration of the pulse. Following the initial NP release (particles 'A'), we observed Al removal from the surface in the form of 6.5 µm-thick column structures (red arrows, **Fig. 3 (a)**) and particles (marked as 'B', **Fig. 2 (b)-(c)**). As indicated by the purple arrows in **Fig. 3 (a)**, these column structures have a rippled surface with a 6.5 µm perturbation wavelength. Such perturbations are often observed in laser induced molten surfaces due to hydrodynamic instabilities.[8, 9]

Fig. 3 (b) shows the Distance-Time (R-t) plot of the column structures and ejected NPs calculated from data shown in **Fig. 2**. Specifically, the R-t plot was deduced from the distance travelled between the target surface and the propagation front, at any given time (pink arrows, **Fig. 2 (c)**). An example of the liquid column propagation at an average speed of 13.5 m/s over 4 µs is shown in the scattering images of **Fig. 3 (b)**. This type of speed was observed in the past for liquid phase expulsion driven by recoil pressure.[9] Therefore, the observation of the rippled surface, combined with the measured propagation speed strongly suggest that the columns are liquid Al exhibiting hydrodynamic instabilities.

The front-propagating particles 'A' already disappeared out of the field of view after 1.4 µs, travelling at velocities of the order of 138 m/s. On the other hand, particles 'B' were ejected at different timescales (> 2 µs) with random velocities between 13.5 m/s and 138 m/s (e.g., 42 m/s, 70 m/s, and 88 m/s, as shown in **Fig. 3 (c-i)** for 2.4 µs). These particles often appeared to be ejected laterally with a periodicity of 6.3 µm (**Fig. 3 (c-ii)**), which is consistent with the perturbation wavelength observed in **Fig. 3 (a)**.

The dimensionless Weber number ($We = \frac{\rho r V^2}{\sigma}$)[15,16], which quantitatively describes the competition between kinetic energy and surface tension, can help elucidate whether the origin of particles 'B' can be attributed to breakup of each liquid branch (or jet) of the hydrodynamically perturbed surface. ρ is the density of liquid Al (2378 kg/m^3)[17], V is the propagation speed, r is the 6.5 µm radius of the jet, and σ is the surface tension of liquid Al (0.9 N/m)[8]. The corresponding We numbers of particles 'B' are 7, 21, and 31, respectively (**Fig. 3 (c-i)**), which fall between those calculated for the liquid Al columns (1.7) and particles 'A' (75), as presented in **Fig. 3 (b)**. Such high values (We > 4) indicate that the kinetic energy is sufficient to overcome the surface tension of the liquid Al, leading to breakup into particles (particles 'B').[15,16]

Figure 2 (d) shows that nearly stagnant liquid mass condensed on top of the liquid columns to a quasi-spherical shape at around 30.4 µs. This accumulated material continues absorbing incoming laser radiation leading to an increase in temperature. Using lumped capacitance analysis (see derivation in **Fig. S1**), the estimated temperature of this accumulated matter (approximated by a 78 µm in diameter spherical particle) would exceed the boiling temperature of Al 2743 K within 5 µs, resulting in fragmentation into microparticles (e.g., the one shown for 35.4 µs, **Fig. 2 (d)**). Such an increase in temperature is sufficient to lead to secondary detonation, which was initiated around 20-50 µs, at a time when enough material had been accumulated over the surface.

ACCEPTED MANUSCRIPT
Applied Physics Letters
This is the author's peer reviewed, accepted manuscript. However, the online version of record will be different from this version once it has been copyedited and typeset.
PLEASE CITE THIS ARTICLE AS DOI: 10.1063/5.0076527
AIP Publishing

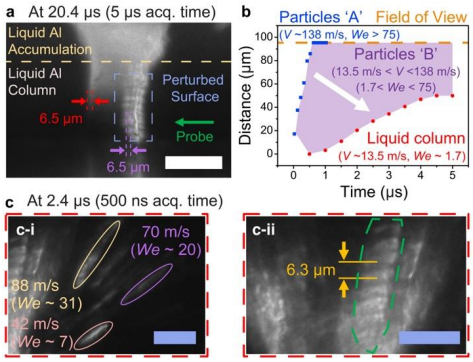

Figure 3. (a) Magnified scattering images at 20.4 μs acquired for 5 μs gate width. The vertically ejecting material has a cylindrical and hollow structure with 6.5 μm in thickness. (b) Distance-Time (R-t) plot of ejected particles and liquid columns calculated from **Fig. 2**. The average speed of particles 'A' is 138 m/s, and that of the liquid columns is 13.5 m/s. V is the propagation velocity, and We is the Weber number. (c) Scattering images at 2.4 μs acquired for 500 ns gate width (magnified view from **Fig. 2 (c)**). The blue scale bar is 25 μm, and the white scale bar is 50 μm.

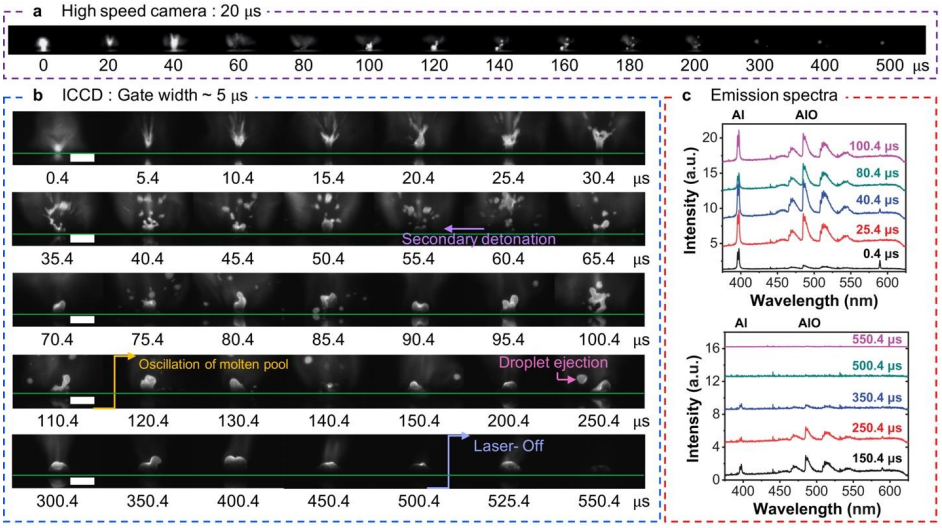

Figure 4. Time-resolved emission images without the probe laser for later times. Material ejection is captured by (a) the high-speed CMOS camera with 20 μs temporal resolution, and (b) the ICCD camera with 5 μs gate width at each time delay. The green line indicates the target surface. The white scale bar is 200 μm. (c) Time-resolved emission spectra measured for 5 μs gate width, corresponding to (b).

Figure 4 shows material ejection at longer times up to 550.4 μs. This figure includes emission imaging data without the probe laser acquired with both the high-speed (**Fig. 4 (a)** and **Video 1**) and ICCD (**Fig. 4 (b)**) cameras, and covers a wider field of view than **Fig. 2** to capture the dynamics of the expanding material ejecta. High speed imaging, offered 20 μs temporal resolution, while the ICCD gate width was increased to 5 μs at each time delay (**Fig. 4 (b)**). **Fig. 4 (c)** shows the corresponding time-resolved emission spectra depicting the evolution of atomic and molecular plasma species for the corresponding emission images in **Fig. 4 (b)**. Prominent atomic Al lines (Al I : 394.4

Applied Physics Letters ACCEPTED MANUSCRIPT
This is the author's peer reviewed, accepted manuscript. However, the online version of record will be different from this version once it has been copyedited and typeset.
PLEASE CITE THIS ARTICLE AS DOI: 10.1063/5.0076527

nm and 396.1 nm)[18] are observed early on (0.4 μs) together with low intensity AlO molecular spectra in the 450-550 nm spectral range, which correspond to the $B^2\Sigma^+ - X^2\Sigma^+$ electronic transition of AlO and the $\Delta\upsilon = 1, 0, -1$ bands.[19] The molecular emission becomes much more pronounced at later times, and such AlO formation at later times (40.4 μs, **Fig. 4 (c)**) coincides temporally with the detonation of liquid Al, as detailed in **Fig. 2**. Interestingly, the emission persistence (lifetime) of these plasmas is much longer (500 μs) than those typical produced by pulsed lasers at atmospheric pressure (~1 μs for femtosecond laser[10,13] and ~10 μs for nanosecond laser[20, 21]). We anticipate that such AlO formation would be suppressed under vacuum or inert conditions due to the lack of ambient oxygen.[22]

After the secondary detonation (> 100.4 μs) described in **Fig 4 (b)**, bulk liquid Al was observed oscillating above the surface with random amplitude and shape. During this period, there was no evidence of subsequent detonation (**Fig. 4 (a)-(b)** and **Video 1**). These oscillations eventually lead to the removal of large droplets with *O*(100 μm) diameter from the liquid pool (250.4 μs, **Fig. 4 (b)**). After completion of the single laser pulse at 500 μs, features remain visible at 525.4 μs with the ICCD system which only captures self-emission. This observation is attributed to still hot remnants on the sample surface, and is not associated with further material removal (**Video 1**).

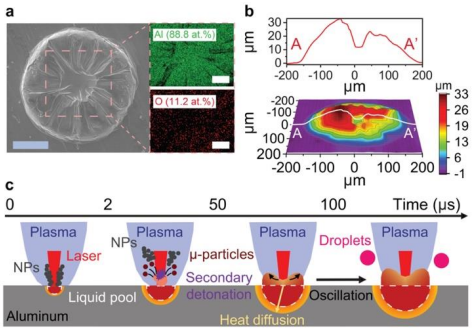

Figure 5. (a) SEM image and EDS analysis of the laser irradiated spot. (b) Surface topography measured by WLI. (c) Summarized ablation dynamics as a function of time. The blue scalebar is 100 μm, and the white scale bar is 50 μm.

Figure 5 (a) shows *ex-situ* characterization of surface morphology after the laser pulse with WLI and SEM, as well as elemental composition with EDS. **Fig. 4 (c)** shows AlO plasma emission evincing oxidation, that is verified by the detection of lower aluminum and higher oxygen content (Al: 88.8 at.% and O: 11.2 at.%) on the laser-irradiated surface, compared to as-received Al (Al: 96 at.%, and O: 4 at.%). **Fig. 5 (b)** shows the corresponding topography measured by a WLI. After single shot irradiation, the area surrounding the irradiated spot protruded above the original surface. This area has a 165 μm radius and a 30 μm height above the original surface, with a 20 μm indentation at the center. As shown in emission imaging (300-550 μs, **Fig. 4 (b)**), the protrusion likely originated from the re-solidified molten liquid pool due to thermal diffusion away from the irradiated spot. This is in accordance with the thermal diffusion length for solid Al which is estimated as ~220 μm in the radial direction for a 500 μs pulse (yellow arrow, **Fig. 5 (c)**). The ablation mechanism associated with the single 500 μs Yb fiber laser pulse is summarized in **Fig. 5 (c)**, based on the experimental results discussed in this Letter.

In conclusion, we analyzed Al ablation mechanisms induced by the Yb fiber laser via time-resolved scattering and emission imaging as well as emission spectroscopy. During the early phase ablation process up to 20 μs, bulk Al was removed from the surface via particle and liquid Al columnar ejection. Secondary detonation occurred when sufficient matter accumulated over the surface (20-50 μs). At later ablation processes (> 100 μs), large droplets were often removed from oscillating molten liquid pool. Atomic Al plasma and Al oxide plasma were observed for entire laser irradiation, suggesting the formation of oxidized Al vapor. We believe that comprehensive understanding of ablation mechanisms by the fiber laser will help selection of laser processing conditions to improve the drilling efficiency and the quality of ablated features.

Supplementary material

See supplementary material for lumped capacitance analysis (Fig. S1) and high-speed video (Video 1).

Applied Physics Letters ACCEPTED MANUSCRIPT

This is the author's peer reviewed, accepted manuscript. However, the online version of record will be different from this version once it has been copyedited and typeset.

PLEASE CITE THIS ARTICLE AS DOI: 10.1063/5.0076527

Acknowledgement

This work was supported DOE NNSA – NA80 - Agreement # CT8405010 FUND CODE 01551 a grant through Sandia National Laboratories. The authors thank Applied Spectra Inc., for use of one of their ICCD cameras.

Data Availability

The data that support the findings of this study are available from the corresponding authors upon reasonable request.

Reference

[1] J. Tu, A.G. Paleocrassas, N. Reeves, and N. Rajule, Opt. Lasers Eng. **55**, 275 (2014).
[2] B.N. Chichkov, C. Momma, S. Nolte, F. Von Alvensleben, and A. Tünnermann, Appl. Phys. A Mater. Sci. Process. **63**, 109 (1996).
[3] D. Paeng, J.H. Yoo, J. Yeo, D. Lee, E. Kim, S.H. Ko, and C.P. Grigoropoulos, Adv. Mater. **27**, 2762 (2015).
[4] S.Z. Khan, Y. Yuan, A. Abdolvand, M. Schmidt, P. Crouse, L. Li, Z. Liu, M. Sharp, and K.G. Watkins, J. Nanoparticle Res. **11**, 1421 (2009).
[5] A. Abdolvand, S.Z. Khan, Y. Yuan, P.L. Crouse, M.J.J. Schmidt, M. Sharp, Z. Liu, and L. Li, Appl. Phys. A **91**, 365 (2008).
[6] C. Kerse, H. Kalaycloğ lu, P. Elahi, B. Çetin, D.K. Kesim, Ö. Akçaalan, S. Yavaş, M.D. Aşlk, B. Öktem, H. Hoogland, R. Holzwarth, and F.Ö. Ilday, Nature **537**, 84 (2016).
[7] B. Adelmann and R. Hellmann, J. Mater. Process. Technol. **221**, 80 (2015).
[8] S. Ly, G. Guss, A.M. Rubenchik, W.J. Keller, N. Shen, R.A. Negres, and J. Bude, Sci. Rep. **9**, 8152 (2019).
[9] Bäuerle, D., 2011. *Laser Processing and Chemistry*. 4th ed. Berlin, Heidelberg: Springer Berlin Heidelberg.
[10] M. Park, J. Jeun, G. Han, and C.P. Grigoropoulos, Appl. Phys. Lett. **116**, 234105 (2020).
[11] C. F. Bohren and D. R. Huffman, Absorption and Scattering of Light by Small Particles (Wiley, 1998).
[12] A.G. Mathewson and H.P. Myers, Phys. Scr. **4**, 291 (1971).
[13] N. Farid, S.S. Harilal, H. Ding, and A. Hassanein, Appl. Phys. Lett. **103**, 191112 (2013).
[14] M. Boueri, M. Baudelet, J. Yu, X. Mao, S.S. Mao, and R. Russo, Appl. Surf. Sci. **255**, 9566 (2009).
[15] W. van Hoeve, S. Gekle, J.H. Snoeijer, M. Versluis, M.P. Brenner, and D. Lohse, Phys. Fluids **22**, 122003 (2010).
[16] S.P. Lin and R.D. Reitz, Annu. Rev. Fluid Mech. **30**, 85 (1998).
[17] J.J. Valencia, P.N. Quested, ASM Handb. Cast. **15**, 468 (2008).
[18] V. Kaufman and W.C. Martin, J. Phys. Chem. Ref. Data **20**, 775 (1991).
[19] X. Bai, V. Motto-Ros, W. Lei, L. Zheng, and J. Yu, Spectrochim. Acta Part B At. Spectrosc. **99**, 193 (2014).
[20] O. Albert, S. Roger, Y. Glinec, J.C. Loulergue, J. Etchepare, C. Boulmer-Leborgne, J. Perrière, and E. Millon, Appl. Phys. A **76**, 319 (2003).
[21] R.E. Russo, X. Mao, J.J. Gonzalez, V. Zorba, and J. Yoo, Anal. Chem. **85**, 6162 (2013).
[22] M.H.A. Shaim and H.E. Elsayed-Ali, J. Appl. Phys. **122**, 203301 (2017).

ACCEPTED MANUSCRIPT

Applied Physics Letters

This is the author's peer reviewed, accepted manuscript. However, the online version of record will be different from this version once it has been copyedited and typeset.

PLEASE CITE THIS ARTICLE AS DOI: 10.1063/5.0076527

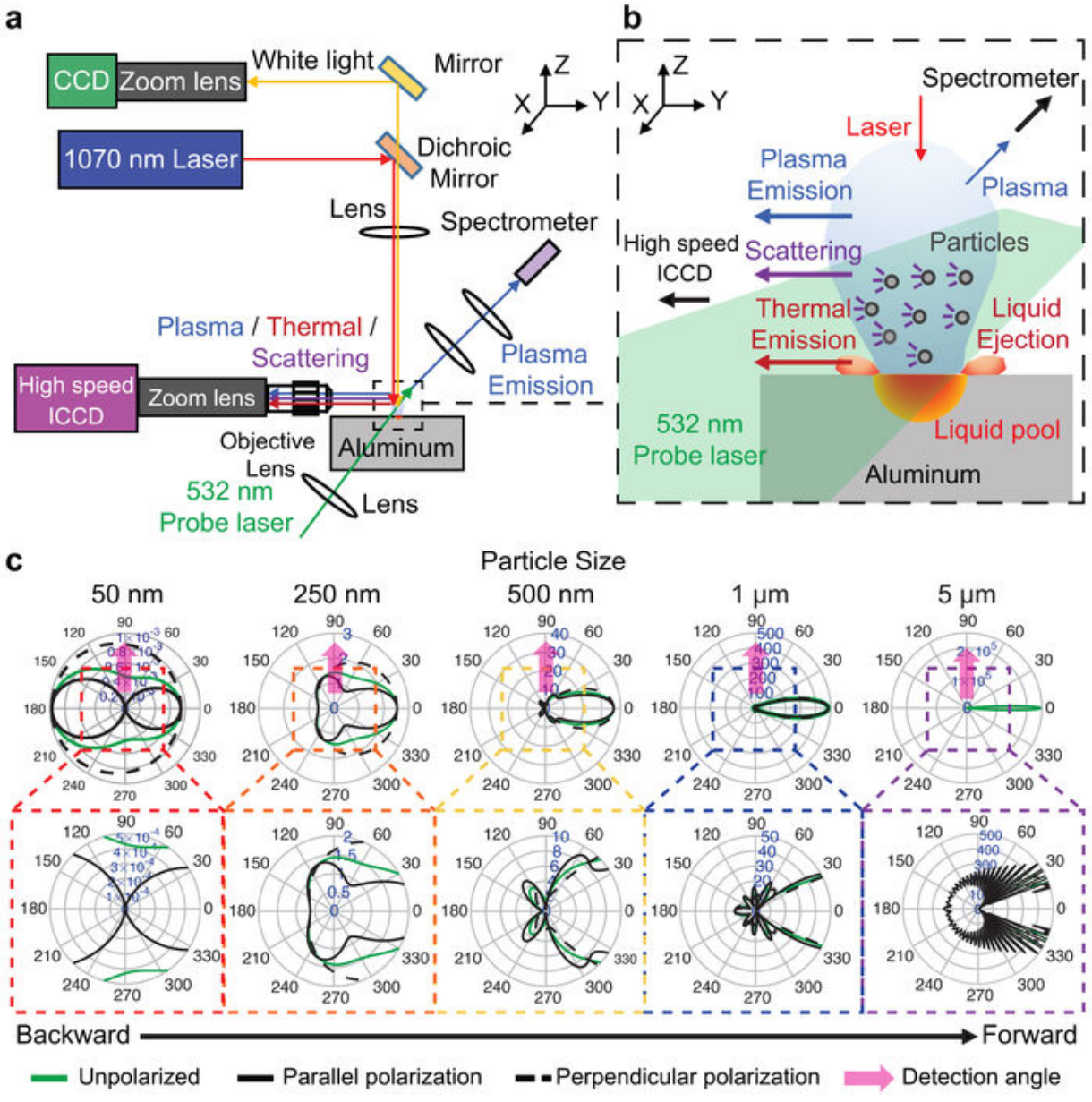

Applied Physics Letters ACCEPTED MANUSCRIPT

This is the author's peer reviewed, accepted manuscript. However, the online version of record will be different from this version once it has been copyedited and typeset.

PLEASE CITE THIS ARTICLE AS DOI: 10.1063/5.0076527

AIP Publishing

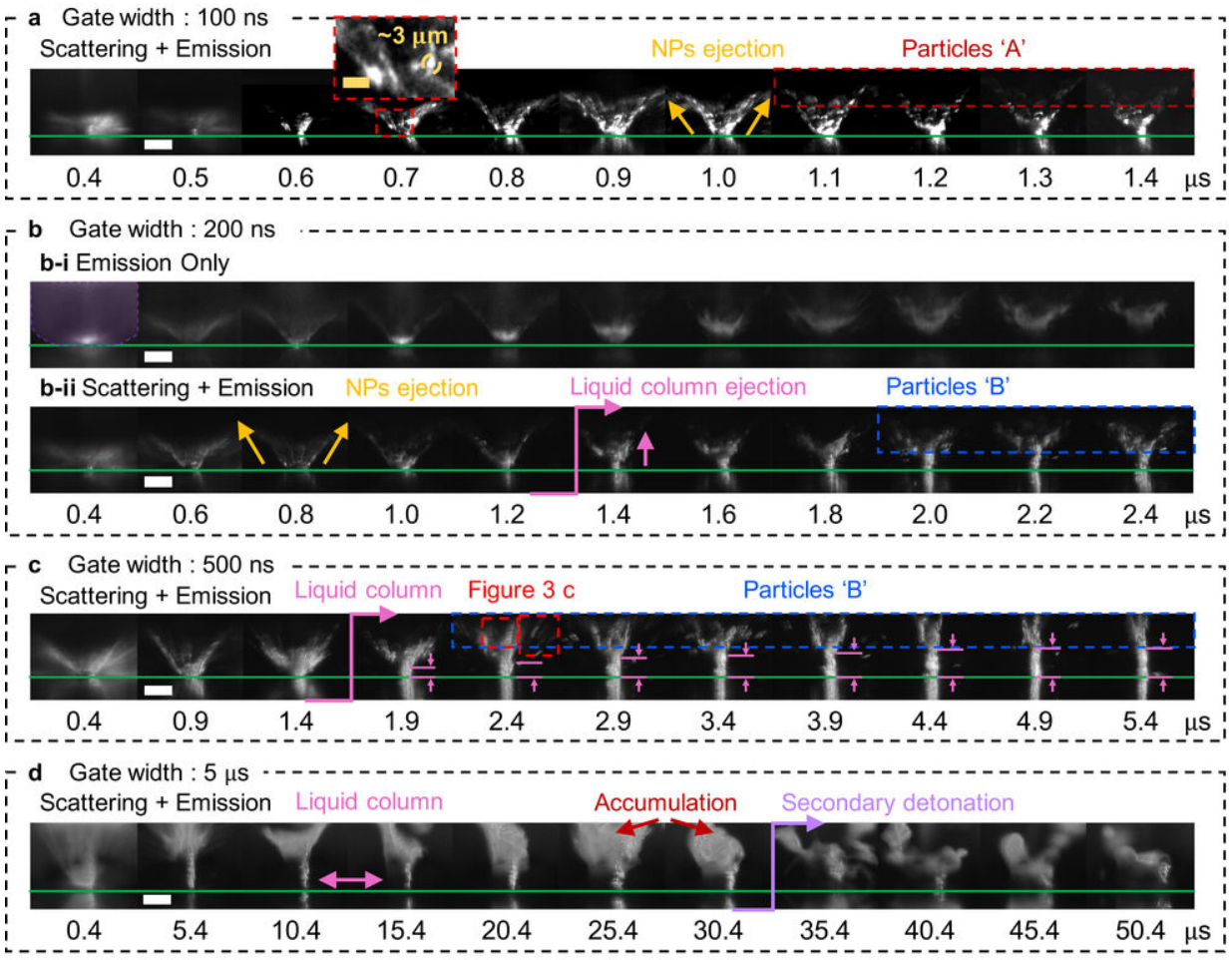

Applied Physics Letters ACCEPTED MANUSCRIPT

This is the author's peer reviewed, accepted manuscript. However, the online version of record will be different from this version once it has been copyedited and typeset.

PLEASE CITE THIS ARTICLE AS DOI: 10.1063/5.0076527

AIP Publishing

AIP Publishing

Applied Physics Letters ACCEPTED MANUSCRIPT

This is the author's peer reviewed, accepted manuscript. However, the online version of record will be different from this version once it has been copyedited and typeset.

PLEASE CITE THIS ARTICLE AS DOI: 10.1063/5.0076527

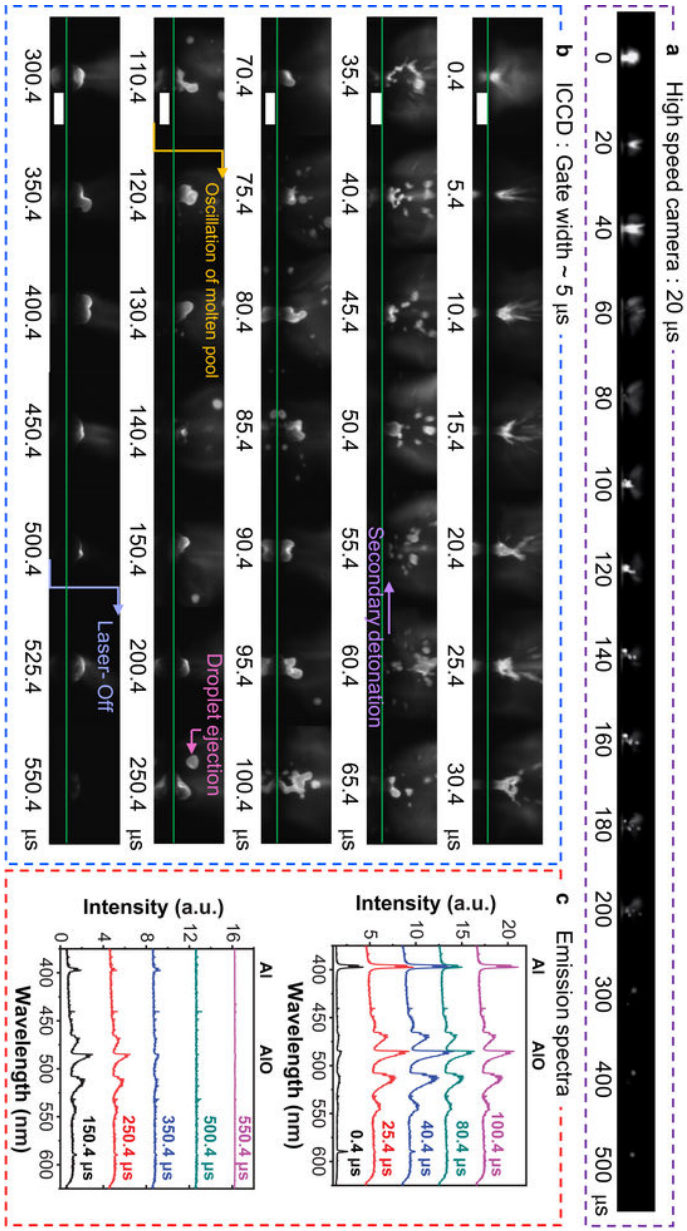

AIP Publishing

Applied Physics Letters ACCEPTED MANUSCRIPT

This is the author's peer reviewed, accepted manuscript. However, the online version of record will be different from this version once it has been copyedited and typeset.

PLEASE CITE THIS ARTICLE AS DOI: 10.1063/5.0076527